coatings

MDPI

Article

The Working Performance and Mechanical Strength of Reactive Powder Concrete with the CO_2 Curing Method on the Surface of Secondary Aluminum Ash

Peng Tang [1], Xin Cai [2], Hui Wang [2,*] and Feiting Shi [3]

[1] School of Municipal and Transportation Engineering, Anhui Water Conservancy Technical College, Hefei 231603, China; pengtang134@aliyun.com
[2] School of Civil Engineering and Geographic Environment, Ningbo University, Ningbo 315000, China; caixin67@aliyun.com
[3] School of Civil Engineering, Yancheng Institute of Technology, Yancheng 224051, China; shifeiting@ycit.cn
* Correspondence: huiwang123@aliyun.com

Abstract: Secondary aluminum ash (SAA) is a common waste that, without reasonable treatment, results in pollution to the environment. A large amount of CO_2 is emitted by human activities every day. If the CO_2 cannot be treated in a timely manner, it will accelerate the greenhouse effect and pollute the environment. The CO_2 curing on the surface of SAA can reduce excess CO_2 emissions while improving the performance of the SAA. The application of CO_2-cured SAA can simultaneously consume the emitted CO_2 and solidify the SAA. In this article, the effect of CO_2-cured secondary aluminum ash on the rheological properties, the initial setting time, the flexural strength (f_t), the compressive strength (f_{cu}) of reactive powder concrete (RPC), and the corresponding dry shrinkage rate (DSR) are investigated. Meanwhile, the capillary water absorption, the chloride ion migration coefficient (CMC), and the carbonization depth of RPC are determined. Scanning electron microscope (SEM) and the X-ray diffraction spectrum curves are selected to reveal the mechanism of the macro performance. Results indicate that CO_2-cured secondary aluminum ash can increase the fluidity and decrease the plastic viscosity of fresh RPC. The initial setting time is increased by the CO_2 curing. CO_2-cured secondary aluminum ash can increase the f_t and f_{cu} by (0%~26.3% and 0% to 68.7%), respectively. The *DSR* is increased by adding secondary aluminum ash with an increasing rate of 0% to 91.3%. The capillary water absorption of RPC increases in the form of a linear function. The CMC and the carbonization depth of RPC are decreased by adding the CO_2-cured secondary aluminum ash with decreasing rates of 0%~46.7% and 0%~45.7%. The CO_2-cured secondary aluminum ash can make the hydration more compact and increased increase the hydration products ($Ca(OH)_2$).

Keywords: CO_2 curing; surface; secondary aluminum ash; rheological properties; dry shrinkage rate; initial setting time; X-ray diffraction spectrum

Citation: Tang, P.; Cai, X.; Wang, H.; Shi, F. The Working Performance and Mechanical Strength of Reactive Powder Concrete with the CO_2 Curing Method on the Surface of Secondary Aluminum Ash. *Coatings* **2023**, *13*, 1377. https://doi.org/10.3390/coatings13081377

Academic Editor: Elena Villa

Received: 13 July 2023
Revised: 31 July 2023
Accepted: 31 July 2023
Published: 5 August 2023

1. Introduction

As a kind of solid waste, secondary aluminum ash (SAA) can pollute the environment if reasonable treatment is not carried out [1–3]. The magnetic separation method, plasma technology, the acid leaching method, and fused salt electrolysis are the main processing methods for the treatment of secondary aluminum ash [4,5]. However, these processing methods are not only inefficient but also cost-ineffective. Therefore, some simple, low-cost, and efficient methods should be adopted to handle this solid waste. The resource utilization of solid waste is a relatively ideal treatment method.

The application of SAA in cement materials is a relatively recognized method. SAA possesses some reactive oxygen species, which can accelerate the hydration process of cement, thus increasing the corresponding mechanical strengths and durability. SAA can be used as an active admixture, which can enhance the cementitious activity, further achieving

the enhancement of the corresponding mechanical strength and durability. The flexural strength (f_t) and the compressive strength (f_{cu}) are increased by rates of 23.1% and 33.4% by adding SAA. Hence, the addition of SAA is advantageous to the performance of the cement matrix [6–8].

RPC is short for reactive powder concrete, which is a kind of high-performance concrete. This cement concrete is composed of cement, mineral admixtures, quartz sand, and some reinforced fibers. The influence of waste fly ash, fly ash, and rice husk ash is able to improve the mechanical strengths and the resistance to chloride erosion. Moreover, the corrosion resistance of reinforced RPC can be improved by adding these solid wastes when NaCl erosion is exerted on the specimens [9–15].

CO_2 curing on raw materials has been proven to make the raw materials more compact and further increase the mechanical strengths of the cement matrix. Witoon et al. have reported that CO_2 curing on the waste fly ash, sludge, and fly ash can improve the corresponding mechanical strengths with these cementitious materials. The f_t and f_{cu} of RPC can be increased by 14.6% and 16.3% with CO_2-cured waste fly ash. On the other hand, CO_2 curing on solid waste can solidify the inner toxic elements and reduce their external emissions [16–22]. Xu et al. [23] found that CO_2 curing on waste fly ash can decrease the release of heavy metals by dozens of times. Moreover, some researchers have pointed out that CO_2-cured steel slag, yellow phosphorus slag, and furnace slag can effectively improve the mechanical strengths of the cement matrix. The flexural strength of cement mortar with CO_2-cured steel slag, yellow phosphorus slag, and furnace slag is 23.6%, 13.8%, and 24.5% higher than that of cement mortar with raw solid waste. Moreover, the corresponding compressive strengths are 21.4%, 14.6%, and 26.7% higher [24–26].

However, the compactness of ordinary cement-based materials is not high, and their inner harmful substances easily seep out. RPC with high compactness can prevent the heavy metals in SAA from leaching. CO_2 curing on SAA can solidify toxic substances in SAA while increasing the mechanical strengths of RPC. However, this method of handling SAA has not been mentioned.

The effect of CO_2-cured SAA on the rheological properties of fresh RPC is measured in this article. The initial setting time, the f_t, and the f_{cu} of RPC are determined. The capillary water absorption of RPC is obtained. The corresponding dry shrinkage rate is measured. The chloride ion migration coefficient (CMC) and carbonization depth are found. The scanning electron microscope (SEM) photos and the X-ray diffraction spectrum curves are obtained to analyze the mechanism of the macro performance. This research can offer an excellent method for better resource utilization of SAA, manufacturing RPC, and dealing with excessive CO_2 emissions. The mechanical strengths and durability of SAA–RPC under various erosive environments are very novel and meaningful, and will be systematically studied in the future.

2. Experimental Section

2.1. Raw Materials

In this study, the initial and final setting times of ordinary Portland cement (OPC) are 98.7 min and 318.1 min, respectively, provided by Zhengzhou Shunbao Cement Co., Ltd., Zhengzhou, China. Fly ash (FA) with a specific surface area of 14–25 m^2/g is selected as a mineral admixture, with a bulk density of 196 kg/m^3 and an average particle size of 0.11–0.17 μm. FA was purchased from Shandong Shunke Building Materials Technology Co., Ltd., Longkou, China. The aluminum ash purchased from Anyang Jiacheng Yenai Co., Ltd., Anyang, China, contains 22% to 50% Al_2O_3 and less than 10% SiO_2. Level S95 blast furnace slag powder (BFS) with a density of 2.88 g/cm^3, activity index above 95%, a specific surface area of 437.1 m^2/g, and a loss on ignition of 2.21% manufactured by Hebei Chuangtian Engineering Materials Co., Ltd., Shijiazhuang, China, is used as another mineral admixture. The quartz sand produced by Xinghongye Calcium Industry Co., Ltd., Changxing, China, has a SiO_2 content of over 99.5% and an apparent density of 2.66 g/cm^3. The aggregates used in this study are three different particle sizes of quartz

sand, with particle sizes ranging from 3.28 to 1.59 mm, 0.82 to 0.31 mm, and 0.31 to 0.19 mm, respectively. The dosage ratio of the three particle sizes is 1:1.5:1. The particle size and compositions of the cementitious materials are shown in Tables 1 and 2. The flowability of fresh RPC is adjusted by polycarboxylate superplasticizer, whose water-reducing rate is 37.8%.

Table 1. The accumulated pass rate of the powder materials (%).

Types	Particle Size/μm						
	0.3	**0.6**	**1**	**4**	**8**	**64**	**360**
OPC	0.12	0.31	2.5	15.6	28.2	93.3	100
BFS	0.045	0.14	3.27	19.36	35.15	98.12	100
FA	31.26	58.47	82.35	100	100	100	100
Quartz sand	0	0	0	0	0.039	23	100
SAA	0.06	0.23	0.62	1.15	3.96	25.7	87.47

Table 2. Chemical composition of the powder materials (%).

Types	SiO_2	Al_2O_3	Fe_xO_y	MgO	CaO	SO_3	K_2O	Na_2O	Ti_2O	Loss on Ignition
OPC	20.9	5.5	3.9	1.7	62.2	2.7	-	-	-	3.1
BFS	33.9	15.0	0.48	9.82	36.7	0.4	3.7	-	-	-
SF	90.7	0.22	0.61	0.24	0.45	0.1	7.6	-	-	-
Quartz sand	99.4	-	0.6	-	-	-	-	-	-	-
SAA	4.6	79.3	3.9	5.7	1.5	-	-	0.9	-	-

2.2. The Manufacturing Process of Specimens

NJ-160A mixer is used for mixing SAA–RPC with a water–binder ratio of 0.2. The dried material is placed in a mixer and mixed at a rotational speed of 60 ± 2 r/min for 2 min. After mixing the material, the solution of water and water reducer is poured into the mixer, and the rotational speed is then increased to 80 ± 2 r/min for 6 min. The freshly mixed slurry is injected with a size of 40 × 40 × 160 mm^3 and 50 × 50 × 50 mm^3 molds. After demolding, the specimens are cured in the standard curing environment ((20 ± 2) °C and relative humidity of 96.2%). The concrete carbonization test box provided by Xianxian Jiantong Test Instrument Sales Department, Cangzhou, China, is used to offer the carbonization environment. The concentration of CO_2 in the concrete carbonization test box is 20%, and the concrete carbonization test box shows a gas pressure of 0.5 MPa. Figure 1 shows the manufacturing process of the RPC samples. The mixing proportions are shown in Table 3.

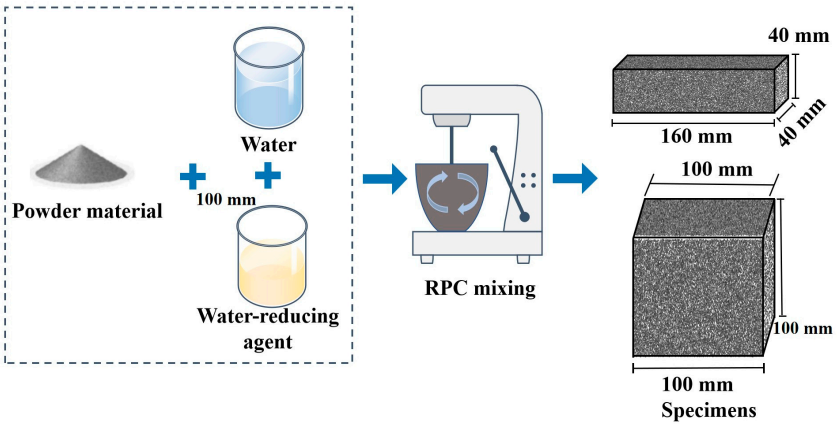

Figure 1. The manufacturing process of RPC with SAA.

Table 3. The mixing proportions of RPC with SAA (kg/m^3).

Water	OPC	SAA	FA	BFS	Quartz Sand	Water-Reducer
243.42	737.74	0	368.82	110.66	973.99	16.23
243.42	737.74	92.23	276.59	110.66	973.99	16.23
243.42	737.74	184.46	184.46	110.66	973.99	16.23
243.42	737.74	276.59	92.23	110.66	973.99	16.23
243.42	737.74	368.82	0	110.66	973.99	16.23

2.3. Measurement of Rheological Properties and Setting Time

An NLD-3CSA mortar dry material fluidity tester is used for the measurement of slump flow of fresh RPC. The yield shear stress of freshly mixed RPC is tested in the experiment; the Huck rotary rheometer used for testing is provided by Shanghai Diguan Industrial Co., Ltd. (Shanghai, China), with a testing speed range of 0 r/min to 30 r/min. The measuring details are described in Sun's research [27]. The measuring process of yield shear stress can be observed in Wang's research [28]. The initial setting time of RPC is measured using a ZKS-100A mortar setting time tester offered by Shanghai Leiyun Testing Instrument Manufacturing Co., Ltd. in Shanghai, China. The measuring process can be found in Chinese standard JGJ70-90 [29]. Figures 2 and 3 show the measuring equipment of rheological properties and setting time.

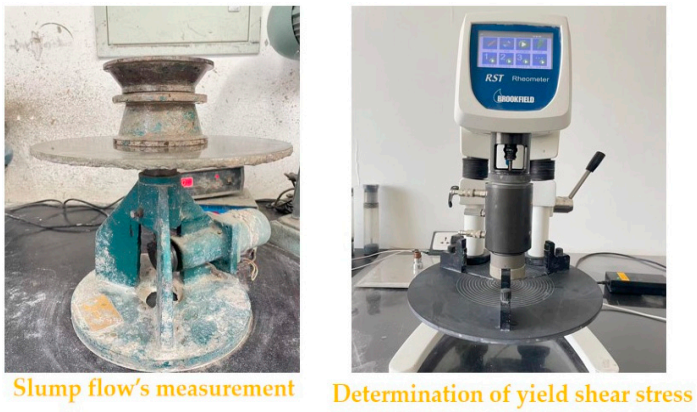

Figure 2. The measuring process of fresh SAA–RPC's rheological parameters.

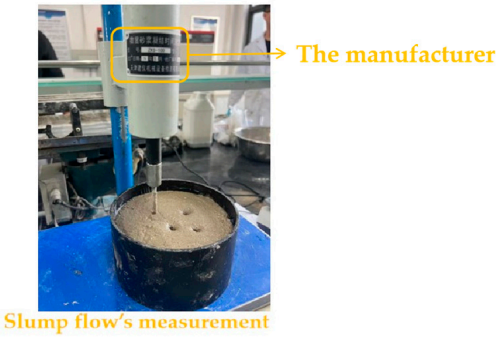

Figure 3. The initial setting time of fresh SAA–RPC.

2.4. The Determination of Mechanical Strengths

The mechanical strength measurement process mainly refers to the Chinese standard GB/T17671-1999 [30] and Zhu's research [31]. In the experiment, the flexural and compressive strength of the samples are mainly collected, and a YAW-300C fully automatic bending and compression testing machine is used to measure these two strengths. Specimens with size of 40 × 40 × 160 mm^3 are used for the determination of flexural and compressive

strengths. The testing speeds for bending strength and compressive strength are 2.4 kN/s and 0.1 kN/s, respectively. The testing process of mechanical strength is shown in Figure 4. Three specimens are used for the measurement of flexural strength. After the specimens are folded into two sections, the six broken samples are moved to the compression clamp to test their compressive strength. After the flexural and compressive experiments, the average values and the error bars' values are obtained to characterize the experiments' accuracy.

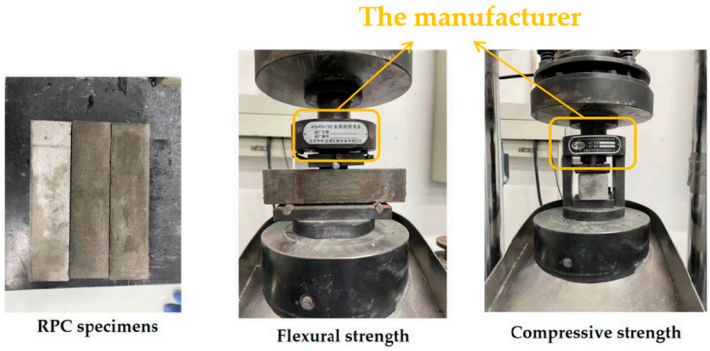

Figure 4. The measurement of SAA–RPC's mechanical strength.

2.5. The Determination of Drying Shrinkage Rate

A micrometer provided by Shenzhen Lide Xinmao Technology Co., Ltd., Shenzhen, China, is used for drying shrinkage rate (*DSR*) testing. *DSR* testing requires the following steps: first, install the sample on the bracket of the multimeter, and then use a micrometer to test the shrinkage value. *DSR* can be obtained by Equation (1).

$$DSR = \frac{L_1 - L_t}{L_1} \quad (1)$$

In Equation (1), L_0 represents the initial length of the specimen, and L means the length of specimen at different curing ages. By this method, the *DSR* is obtained. The measurement of *DSR* is shown in Figure 5.

Figure 5. The testing process of *DSR* for SAA–RPC.

2.6. Capillary Water Absorption

The capillary water absorption (CA) is measured with the specimens of size Φ100 mm × 100 mm. The vacuum oven is used to dry the specimens. The around sides of the specimens are coated with epoxy resin. After the epoxy resin is hardened, the specimens are moved for the measurement of capillary water absorption. The bottom surface is immersed in distilled water, and the mass of specimens is measured every ten minutes.

2.7. The Measurement of CMC

The specimens with size of Φ100 mm × 50 mm are used to measure the CMC. The NELD-CCM540 cement chloride ion diffusion coefficient tester provided by Shanghai Meiyu Instrument Technology Co., Ltd., Shanghai, China, is used for testing the CMC.

2.8. The Measurement of Carbonation Depth

The specimens with size of 100 mm × 100 mm × 100 mm are used for the measurement of the carbonation depth (D_c). The specimens are placed in a carbonization curing box with a CO_2 concentration of 20% for 90 days, and then the carbonation depth is measured. The Chinese standard GB/T 50082-2009 is the reference for the determinations of CMC and carbonation depth [32]. Six specimens are used for the experiments to test the DSR, the CA, the CMC, and the D_c. After the measurement, the average values are considered as the tested results.

2.9. The Scanning Electron Microscopy and XRD Experiments

The samples are removed from the inner parts of the specimen. The particle size range of the sample is 0.5~3 mm. All samples are dried in a Li Chen vacuum drying chamber provided by China Experimental Instrument Sales Center, Beijing, China. Subsequently, the dried sample is moved to a vacuum spraying chamber for gold spraying. The SEM photos of the samples are observed with Zeiss Scanning electron microscope. The remaining samples are crushed into powder in a mortar. The powder sample is placed in a TD-3500 Diffractometer (purchased from Wuxi Lingen Electromechanical Equipment Co., Ltd., Wuxi, China) to obtain the X-ray diffraction spectrum.

3. Results and Discussions

3.1. The Rheological Parameters of SAA–RPC

The slump flow of fresh RPC is shown in Figure 6. In Figure 6, the slump flow increases with the increasing dosages of CO_2-cured SAA. As described in Li's research, CO_2 curing can promote the reaction between alumina and CO_2, forming $Al_2(CO_3)_3$ and decreasing the pores' inner SAA. The decreased pores can decrease the absorption of free water in the fresh RPC [33,34]. Therefore, the slump flow is increased by adding an amount of SAA. The growth rate ranges from 0% to 23.04%. Moreover, the error bars are less than 2.5% of the slump flow, indicating the accuracy of the experiment.

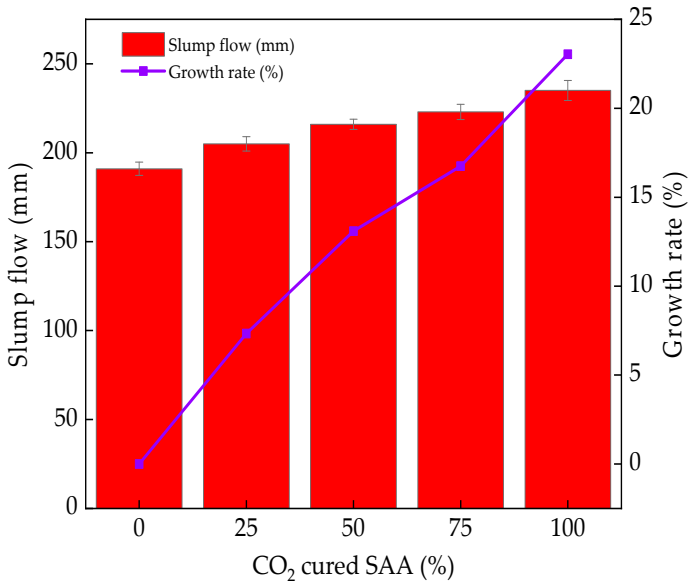

Figure 6. The slump flow of fresh SAA–RPC.

Figure 7 shows the yield shear stress of fresh RPC. As illustrated in Figure 7, the yield shear stress decreases with the increasing dosages of CO_2-cured SAA. Liu et al. found that CO_2 curing on SAA can decrease its ability to adsorb free water, thus increasing the fluidity of fresh RPC [35]. As described in previous research, the yield shear stress of fresh RPC shows a negative relationship with that of slump flow [36,37]. Therefore, the yield shear stress of fresh RPC is reduced by adding the CO_2-cured SAA. The reduction rate of the yield shear stress varies from 0% to 31.96%. Meanwhile, the error bars' values are 1.0%~2.2%, showing the accuracy of the measuring results.

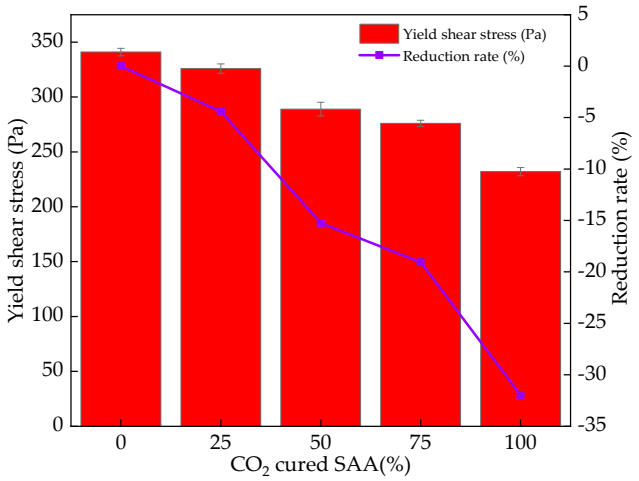

Figure 7. The yield shear stress of fresh SAA–RPC.

3.2. The Initial Setting Time of SAA–RPC

The initial setting time of fresh RPC is illustrated in Figure 8. It can be found that the initial setting time of fresh RPC increases by adding CO_2-cured SAA, due to how the CO_2 curing can increase the amount of $Al_2(CO_3)_3$ and decrease the pores' inner SAA. The $Al_2(CO_3)_3$ adsorbs on the surface of hydration products, increasing the initial setting time of RPC [38]. The growth rate of RPC's initial setting time ranges from 0% to 117.3%. Additionally, the error bars' values are lower than 3.1% of the initial setting time. Therefore, the results of this experiment are accurate.

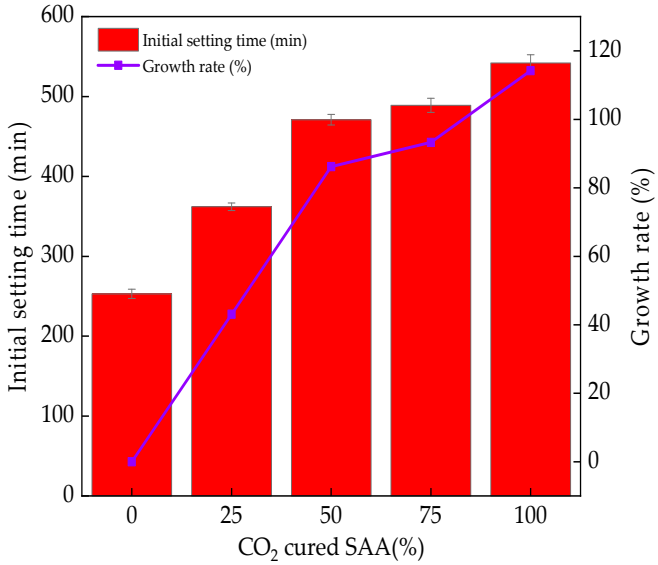

Figure 8. The initial setting time of fresh SAA–RPC.

3.3. The Mechanical Strengths of SAA–RPC

The flexural strength (f_t) of RPC is observed in Figure 9. The f_t of specimens cured for 1 day, 7 days, and 28 days show an ascending trend when adding CO_2-cured SAA. CO_2 curing on SAA can increase the amount of $Al(OH)_3$, thus increasing the f_t of RPC. The growth rates of the f_t are 0%~26.3%. The curing age demonstrates a positive effect on the f_t of RPC. This is attributed to the increased hydration degree of cement [39–41]. The values of the error bars are less than 2.41% of the f_t.

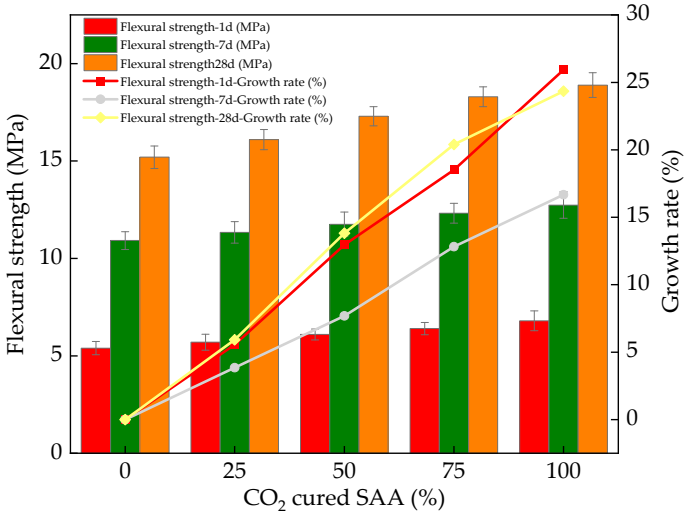

Figure 9. The f_t of SAA–RPC.

The compressive strength (f_{cu}) of RPC is shown in Figure 10. The f_{cu} of RPC increases with the increasing dosages of CO_2-cured SAA. The f_{cu} of RPC is increased by the increasing curing age. The growth rate of RPC's f_{cu} ranges from 0% to 68.7%. The error bars' values are less than 3.76% of the f_{cu}, which indicates the accuracy of the experiment.

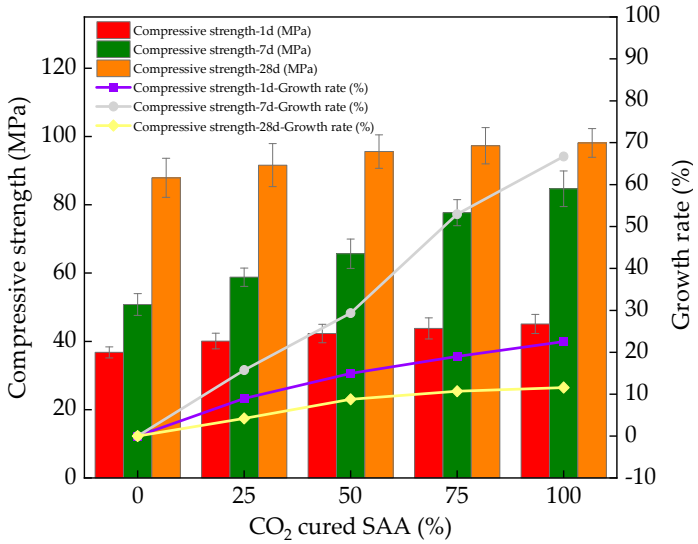

Figure 10. The f_{cu} of SAA–RPC.

3.4. The DSR of SAA–RPC

The *DSR* of RPC is observed in Figure 11. The *DSR* of RPC increases with the increasing dosages of CO_2-cured SAA. The *DSR* of RPC is increased by the increasing curing age. The hydration of cement is increased by adding CO_2-cured SAA, as it decreases the free water and increases the *DSR* of RPC. The increasing rate of the *DSR* ranges from 0% to 91.3%.

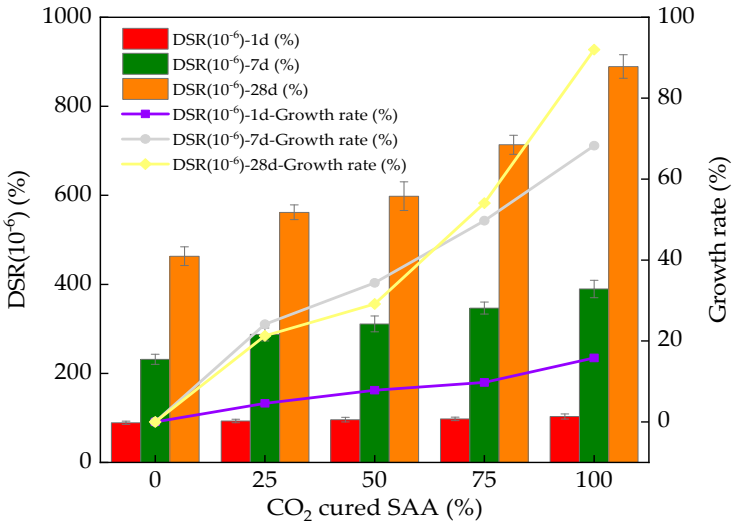

Figure 11. The *DSR* of SAA–RPC.

3.5. Capillary Water Absorption

Figure 12 shows the capillary water absorption of RPC with different dosages of CO_2-cured SAA. The mass of absorbed water decreases in the form of a linear function with the immersion time. The fitting degrees of the functions are higher than 0.95, which confirms the accuracy of the fitting results. As found in Figure 12, the addition of CO_2-cured SAA can decrease the mass rate of absorbed water that increases with the immersion time, due to the improved compactness caused by the CO_2-cured SAA.

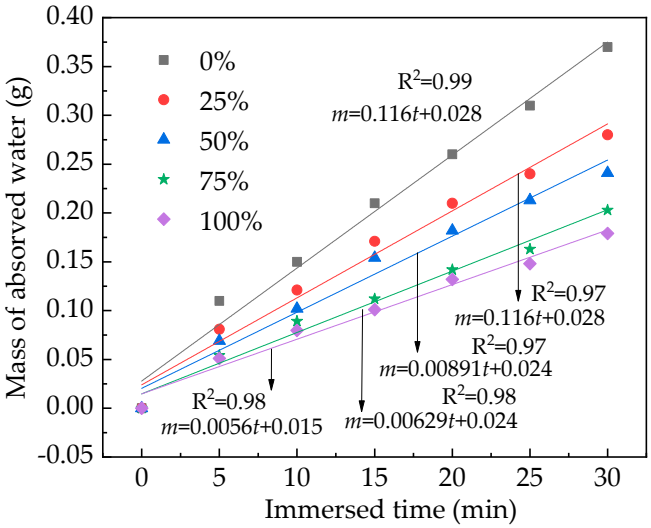

Figure 12. The capillary water absorption of SAA–RPC.

3.6. The CMC of RPC

The CMC of RPC is shown in Figure 13. The CMC of RPC ranges from 1.1×10^{-12} to 2.1×10^{-12}. This is ascribed to the fact that open pores exist in the RPC. Therefore, the chloride ions migrate along open pores under the action of an electric field, leading to an increase in the CMC. Moreover, as illustrated in Figure 13, the CMC of RPC decreases with increasing dosages of CO_2-cured SAA. The decreasing rate of the CMC ranges from 0% to 46.7% due to the fact that the CO_2-cured SAA can increase the hydration degree of cement, thus improving the compactness of RPC [42–44]. Consequently, the CMC of RPC is decreased by adding the CO_2-cured SAA. The error bars' values of the CMC are lower than the real values of the CMC, which confirm the accuracy of the CMC's testing results.

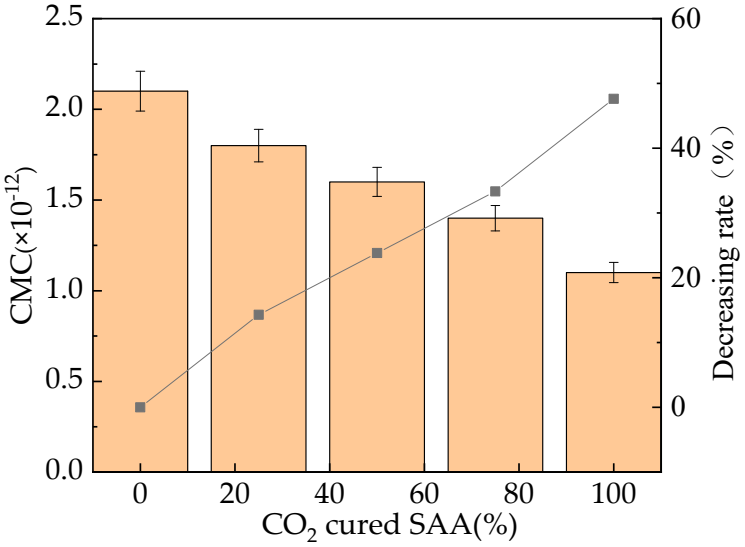

Figure 13. The CMC of SAA–RPC.

3.7. The Carbonization Depth of RPC

Figure 14 shows the carbonization depth of RPC. As observed in Figure 14, the carbonization depth decreases with the increasing dosages of CO_2-cured SAA. This is ascribed to the fact that the CO_2-cured SAA can improve the compactness of RPC [45,46]. Therefore, the migration rate of CO_2 in RPC becomes slow, leading to a decrease in the carbonization depth of RPC. The decreasing rate of carbonization depth by the CO_2-cured SAA ranges from 0% to 45.7%, with the mass ratio of CO_2-cured SAA increasing from 0% to 100%. The error bars are lower than 7.8% of the real values of the carbonization depth, indicating the accuracy of the experimental results.

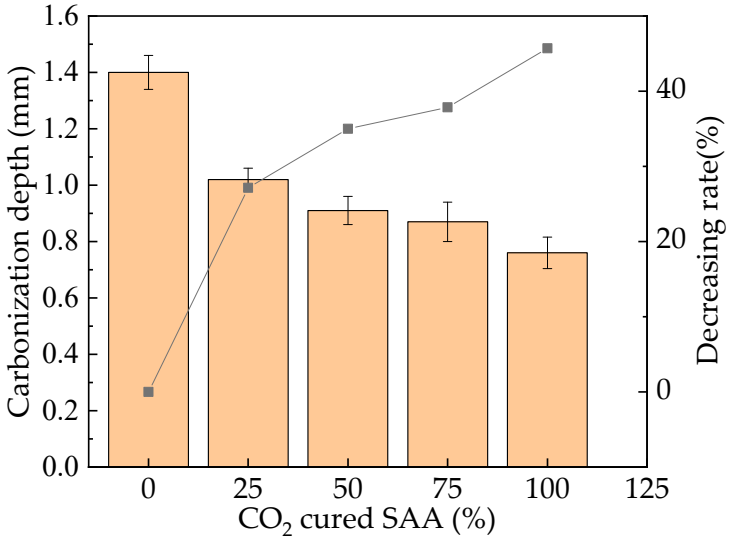

Figure 14. The carbonization depth of SAA–RPC.

3.8. Microscopic Analysis

The SEM photos of RPC are shown in Figure 15. The specimens are cured in the standard curing environment for 28 days. As observed in Figure 15, fibrous hydration products are found when the mass ratios of CO_2-cured SAA are 0% and 50%, respectively. The fibrous hydration products are decreased by the increasing dosages of CO_2-cured SAA. This indicates the fact that the addition of CO_2-cured SAA can inhibit the appearance of fibrous hydration products. Moreover, the increased CO_2-cured SAA can improve the

compactness of the RPC. Therefore, the mechanical strengths are improved by adding the CO_2-cured SAA.

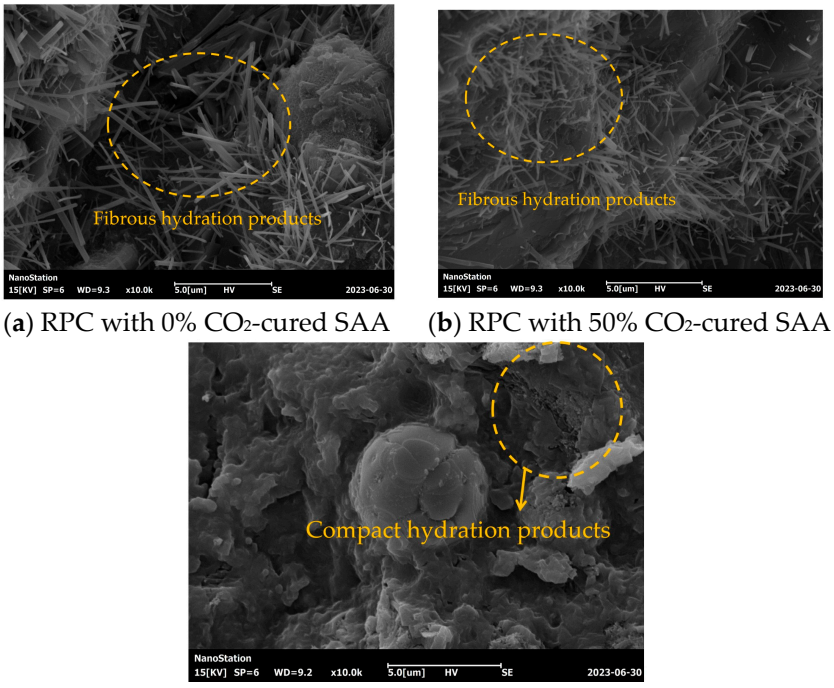

(**a**) RPC with 0% CO_2-cured SAA (**b**) RPC with 50% CO_2-cured SAA

(**c**) RPC with 100% CO_2-cured SAA

Figure 15. The SEM of RPC with CO_2-cured SAA.

The XRD curves are exhibited in Figure 16. As shown in Figure 16, the crystals' diffraction peaks of calcium silicate (C_3S), dicalcium silicate (C_2S), silica (SiO_2), calcium hydroxide (CH), and aluminum oxide (Al_2O_3) are observed. As found in Figure 16, the crystals' diffraction peaks of calcium silicate, dicalcium silicate, silica, and aluminum oxide are decreased by adding CO_2-cured SAA, while the crystals' diffraction peaks of calcium hydroxide are increased. This is attributed to the fact that the addition of CO_2-cured SAA can improve the hydration degree of cement, thus decreasing the content of calcium silicate, dicalcium silicate silica, and aluminum oxide and increasing the content of calcium hydroxide.

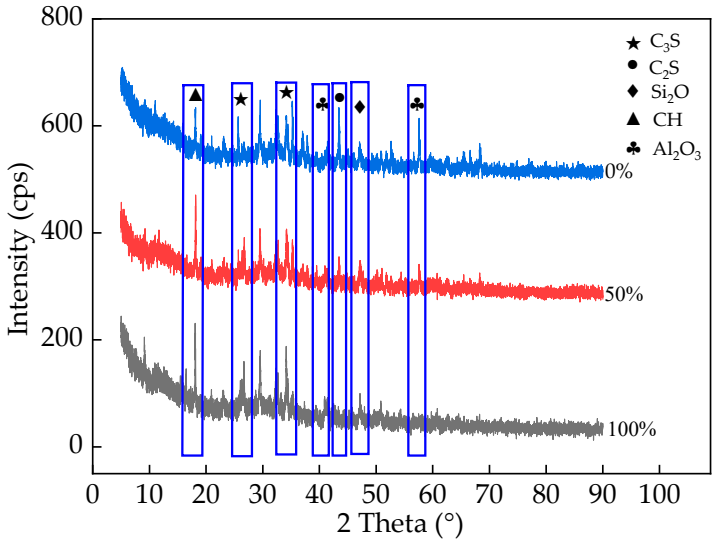

Figure 16. The XRD of RPC with CO_2-cured SAA.

4. Conclusions

The influence of CO_2-cured SAA on the working properties, the mechanical strengths, and the durability were investigated. The research results are summarized as follows.

Due to the reduction in SAA porosity caused by carbonization, the slump flow of fresh RPC is increased, and the corresponding plastic viscosity is decreased by adding CO_2-cured SAA. The slump flow increases by 0%~23.04%, and the plastic viscosity decreases by 0%~31.96%. The initial setting time is increased by CO_2-cured SAA, with an increasing rate of 0%~117.3%.

The addition of SAA can improve the mechanical strengths of RPC by increasing the SAA's activity and reducing the corresponding porosity. The flexural and compressive strengths of RPC are increased with the increasing rates of the CO_2-cured SAA, with the increasing rates of 0%~26.3% and 0%~68.7%, respectively. The CO_2-cured SAA can increase the *DSR* of RPC with an increasing rate of 0%~91.3%. The capillary water absorption of RPC increases in the form of a linear function.

Following the research on RPC's durability, it was found that the addition of CO_2-cured SAA can decrease the CMC and the carbonization depth of RPC by rates of 0%~46.7% and 0%~45.7%, respectively.

As obtained from the SEM results, the CO_2-cured SAA can decrease the production of needle-shaped hydration products, increasing the compactness of hydration products. The $Ca(OH)_2$ crystals are increased by the addition of CO_2-cured SAA.

This study proved that the CO_2-cured SAA can effectively improve the mechanical strengths of RPC. The application of CO_2-cured SAA in RPC can increase the strength of RPC while reducing its production cost and alleviating environmental pollution.

The effect of CO_2-cured SAA on the durability of RPC under various erosive environments needs to be investigated in the future.

Author Contributions: Conceptualization, H.W. and P.T.; methodology, X.C.; software, H.W.; validation, H.W., P.T. and X.C.; formal analysis, F.S.; investigation, F.S.; resources, H.W.; data curation, X.C.; writing—original draft preparation, P.T.; writing—review and editing, P.T.; visualization, P.T.; supervision, F.S.; project administration, P.T.; funding acquisition, F.S. All authors have read and agreed to the published version of the manuscript.

Funding: Zhejiang Provincial Natural Science Foundation [LY22E080005] and Ningbo Natural Science Foundation Project (2023J086).

Institutional Review Board Statement: Not applicable.

Informed Consent Statement: Not applicable.

Data Availability Statement: Not applicable.

Conflicts of Interest: The authors declare no conflict of interest.

References

1. Ozerkan, N.G.; Maki, O.L.; Anayeh, M.W.; Tangen, S. The effect of aluminium dross on mechanical and corrosion properties of concrete. *Int. J. Innov. Res. Sci. Eng. Technol.* **2014**, *3*, 9912–9922.
2. David, O.; Opeyemi, J.; Adekunle, M.; Babatunde, F. Influence of secondary aluminum dross (SAD) on compressive strength and water absorption capacity properties of sandcrete block. *Cogent Eng.* **2019**, *6*, 1608687.
3. Panditharadhya, B.J.; Sampath, V.; Shankar, A.U.R. Mechanical properties of pavement quality concrete with secondary aluminium dross as partial replacement for ordinary portland cement. *Mater. Sci. Eng.* **2018**, *431*, 032011. [CrossRef]
4. Busari, A.; Joseph, F.; Ajayi, S.; Alayande, T.; Nwachukwu, J. Index properties of aluminum dross modified pavement geo-material. *J. Phys.* **2019**, *1378*, 022102. [CrossRef]
5. Satish, R.; Neeraja, D. Mechanical and durability aspects of concrete incorporating secondary aluminium slag. *Resour.-Effic. Technol.* **2016**, *2*, 225–232.
6. Ewais, E.M.M.; Khalil, N.M.; Amin, M.S. Utilization of aluminum sludge and aluminum slag (dross) for the manufacture of calcium aluminate cement. *Ceram. Int.* **2009**, *35*, 3381–3388. [CrossRef]
7. Zhang, Y.; Guo, C.H. Effects of AlN hydrolysis on fractal geometry characteristics of residue from secondary aluminium dross using response surface methodology. *Trans. Nonferr. Metal. Soc.* **2018**, *28*, 2574–2581. [CrossRef]

8. Arimanwa, J.I.; Onwuka, D.O. Prediction of the Compressive Strength of Aluminum Waste–Cement Concrete Using Scheffe's Theory. *Mater. Sci.* **2012**, *24*, 177–183. [CrossRef]
9. Ren, Y.C.; Wu, F.H.; Qu, G.F. Extraction and preparation of metal organic frameworks from secondary aluminum ash for removal mechanism study of fluoride in wastewater. *J. Mater. Res. Technol.* **2023**, *23*, 3023–3034. [CrossRef]
10. Zhang, J.J.; Liu, B. Theoretical and experimental on the thermodynamic, kinetic and phase evolution characteristics of secondary aluminum ash. *J. Mater. Res. Technol.* **2022**, *19*, 3857–3866. [CrossRef]
11. Zhang, P.B.; Zhu, X.Y.; Jin, Q. Exergoeconomic and exergoenvironmental analyses of a promising alumina extraction process from secondary aluminum dross in China. *J. Environ. Chem. Eng.* **2023**, *11*, 109658. [CrossRef]
12. Trinet, Y. The influence of aluminum dross on mechanical and corrosion properties of cement paste: PART I. *Eng. Technol.* **2019**, *10*, 192–201.
13. Zhang, Y.B.; Lin, K.; Su, Z.J. Self-driven hydrolysis mechanism of secondary aluminum dross (SAD) in the hydrometallurgical process without any additives. *Chem. Eng. J.* **2023**, *466*, 143141. [CrossRef]
14. Ayobami, B.; Jacques, S.; Williams, K. Data on the engineering properties of aluminum dross as a filler in asphalt. *Data Brief* **2020**, *31*, 105934.
15. Gireesh, M.; Sujay, R.; Sreedhara, B.M.; Manu, D.S. Investigation of concrete produced using recycled aluminium dross for hot weather concreting conditions. *Resour.-Effic. Technol.* **2016**, *2*, 68–80.
16. Witoon, T.; Numpilai, T.; Nijpanich, S.; Chanlek, N.; Kidkhunthod, P.; Cheng, C.K.; Ng, K.; Vo, D.-V.N.; Ittisanronnachai, S.; Wattanakit, C.; et al. Enhanced CO_2 hydrogenation to higher alcohols over K-Co promoted In_2O_3 catalysts. *Chem. Eng. J.* **2022**, *431*, 133211. [CrossRef]
17. Sharma, R.; Kim, H.; Pei, J.; Jang, J.G. Dimensional stability of belite-rich cement subject to early carbonation curing. *J. Build. Eng.* **2023**, *63*, 105545. [CrossRef]
18. Peng, L.; Yang, J.; Wang, H.; Jin, X. The Influence of CO_2 Curing on the Mechanical Performance and the Corresponding Chloride Ion Resistance of Alkali-Activated Compound Mineral Admixtures. *Coatings* **2022**, *12*, 1920. [CrossRef]
19. Khan, R.I.; Ashraf, W.; Olek, J. Amino acids as performance-controlling additives in carbonation-activated cementitious materials. *Cem. Concr. Res.* **2021**, *147*, 106501. [CrossRef]
20. Siddique, S.; Naqi, A.; Jang, J.G. Influence of water to cement ratio on CO_2 uptake capacity of belite-rich cement upon exposure to carbonation curing. *Cem. Concr. Compos.* **2020**, *111*, 103616. [CrossRef]
21. Liang, J.; Zhu, H.; Chen, L.; Qinglin, X.; Ying, G. Rebar corrosion investigation in rubber aggregate concrete via the chloride electro-accelerated test. *Materials* **2019**, *12*, 862. [CrossRef] [PubMed]
22. Ogawa, Y.; Bui, P.T.; Kawai, K.; Sato, R. Effects of porous ceramic roof tile waste aggregate on strength development and carbonation resistance of steam-cured fly ash concrete. *Construct. Build. Mater.* **2020**, *236*, 117462. [CrossRef]
23. Xu, F.; Chang, R.; Zhang, D.; Liang, Z.; Wang, K.; Wang, H. Improvement of CO_2-Cured Sludge Ceramsite on the Mechanical Performances and Corrosion Resistance of Cement Concrete. *Materials* **2022**, *15*, 5758. [CrossRef]
24. Song, Q.F.; Guo, M.Z.; Wang, L. Use of steel slag as sustainable construction materials: A review of accelerated carbonation treatment. *Resour. Conserv. Recycl.* **2021**, *173*, 105740. [CrossRef]
25. Hamideh, M.; Shao, X.; Kim, H.M. Enhancement of early age cementitious properties of yellow phosphorus slag via CO_2 aqueous carbonation. *Cem. Concr. Compos.* **2022**, *133*, 104702.
26. Xu, B.; Yi, Y.L. Treatment of ladle furnace slag by carbonation: Carbon dioxide sequestration, heavy metal immobilization, and strength enhancement. *Chemosphere* **2021**, *287*, 132274. [CrossRef] [PubMed]
27. Sun, H.; Shi, F.; Wang, H. Influence of Citric Acid on the Fundamental Properties of CO_2 Cured Magnesium Oxysulfate Paste. *Materials* **2023**, *16*, 1315. [CrossRef]
28. Wang, J.; Wang, S.; Wang, H.; He, Z. Influence of Ceramsite with Assembly Unit of Sludge and Excavated Soil on the Properties of Cement Concrete. *Materials* **2022**, *15*, 3164. [CrossRef]
29. *JGJ/T 70-2009*; Standard for Test Method of Basic Properties of Construction Mortar. Ministry of Housing and Urban-Rural Development of the People's Republic of China: Beijing, China, 2009.
30. *GB/T 17671-1999*; Method of Testing Cements-Determination of Strength. The State Bureau of Quality and Technical Supervision: Beijing, China, 1999.
31. Zhu, X.H.; Yang, J.Z.; Yang, Y.F. Pyrometallurgical process and multipollutant co-conversion for secondary aluminum dross: A review. *J. Mater. Res. Technol.* **2022**, *21*, 1196–1211. [CrossRef]
32. *GB/T50082-2009*; Standard for Test Method of Long-Term Performance and Durability of Ordinary Concrete. General Administration of Quality Supervision, Inspection and Quarantine of the People's Republic of China: Beijing, China, 2009.
33. Haneef, S.M.; Harish, P. An Experimental Investigation on Use of Secondary Aluminium Dross in Cement Concrete. *Eng. Technol.* **2016**, *2*, 204–207.
34. Li, P.; Guo, M.; Zhang, M.; Teng, L.D. Leaching Process Investigation of Secondary Aluminum Dross: The Effect of CO_2 on Leaching Process of Salt Cake from Aluminum Remelting Process. *Metall. Mater. Trans. B* **2012**, *43*, 1220–1230. [CrossRef]
35. Liu, W.Z.; Teng, L.M. CO_2 mineral carbonation using industrial solid wastes: A review of recent developments. *Chem. Eng. J.* **2021**, *416*, 129093. [CrossRef]
36. Han, F.H.; Pu, S.C.; Zhou, Y. Effect of ultrafine mineral admixtures on the rheological properties of fresh cement paste: A review. *J. Build. Eng.* **2022**, *51*, 104313. [CrossRef]

37. Francisco, J.R. Rheological Behavior of Fresh Cement Pastes. *Fluids* **2018**, *3*, 106.
38. Yuan, L.; Qu, G.F. Reuse of secondary aluminum ash: Study on removal of fluoride from industrial wastewater by mesoporous alumina modified with citric acid. *Environ. Technol. Innov.* **2022**, *28*, 102868.
39. Li, T.X.; Mohamed, H.; Kazunori, K.; Kozo, S. Performance of secondary aluminum melting: Thermodynamic analysis and plant-site experiments. *Energy* **2006**, *31*, 1769–1779. [CrossRef]
40. Li, Z.B.; Li, H.Q.; Huang, X.Z.; Wu, W.F. Removal of nitrides and fluorides from secondary aluminum dross by catalytic hydrolysis and its mechanism. *Heliyon* **2023**, *9*, e12893. [CrossRef]
41. Huang, X.L.; Mahendranath, A.; Robert, F. Characterization of salt cake from secondary aluminum production. *J. Hazard. Mater.* **2014**, *273*, 192–199. [CrossRef]
42. Mostafa, M.; Ali, A. A promising green process for synthesis of high purity activated-alumina nanopowder from secondary aluminum dross. *J. Clean. Prod.* **2018**, *179*, 93–102.
43. Elseknidy, M.; Salmiaton, A. A Study on Mechanical Properties of Concrete Incorporating Aluminum Dross, Fly Ash, and Quarry Dust. *Sustainability* **2020**, *12*, 9230. [CrossRef]
44. Nduka, D.; Ede, A. Mechanical and Water Absorption Properties of Normal Strength Concrete (NSC) Containing Secondary Aluminum Dross (SAD). *Int. J. Eng. Res. Afr.* **2020**, *47*, 1–13. [CrossRef]
45. Javali, S.; Chandrashekar, A.R.; Naganna, S.R.; Manu, D.S. Eco-concrete for sustainability: Utilizing aluminum dross and iron slag as partial replacement materials. *Clean. Technol. Environ. Policy* **2017**, *19*, 2291–2304. [CrossRef]
46. Noori, A.N.; Aliewi, J.M.; Salman, H.K.; Numan, H.A. Investigation of lightweight structural materials produced using aluminum scraps with cement mortar. *J. Appl. Eng. Sci.* **2021**, *19*, 252–257.